#### **NURETH14-604**

# MODELING OF TIME-AVERAGED FILM THICKNESS DISTRIBUTION DOWNSTREAM OF BWR FUNCTIONAL SPACERS

M. Damsohn<sup>1</sup> and H.-M. Prasser<sup>1</sup>

<sup>1</sup> ETH Zurich, Switzerland
damsohn@lke.mavt.ethz.ch, prasser@lke.mavt.ethz.ch

#### **Abstract**

Functional spacers play an important role for the annular steam-water flow in boiling water reactors. They are designed to enhance droplet deposition and therefore delay dryout by sustaining the liquid film. Spacers also have an impact on the liquid film thickness on the fuel rod by their effect on the velocity field in the gas core of the flow. This work presents a CFD-based approach to predict the film thickness distribution in proximity of functional spacers based on a two-dimensional mass conservation equation for the liquid film coupled to a steady-state RANS simulation of the gas flow field. The model is validated by experiments with highly resolved film thickness data. For the experiments the gas flow rate, the liquid flow rate, the gas density and the spacer shape are varied. The model and experiments are in good agreement in regard to film thickness distributions downstream of spacers. A model sensitivity analysis shows the key parameters of the model and the potential for future development. The model aims to contribute to the development methodology of functional spacer optimization.

#### Introduction

In the upper part of boiling water reactors the flow regime is dominated by a steam-water droplet flow with liquid films on the nuclear fuel rod, the so called (wispy) annular flow regime. The film thickness and liquid flow rate distribution around the fuel rod play an important role especially in regard to dryout, which is the main phenomenon limiting the thermal power of a fuel assembly in boiling water reactors. Functional spacers with different vane shapes have been used in the last decades to enhance droplet deposition and thus create more favorable conditions for the heat removal.

The prediction of dryout is desirable for the optimization of fuel bundles. Mostly empirical models are found throughout literature, to predict the dryout location, usually based on simplified one-dimensional models for each subchannel e.g. [11]. Recently CFD starts to play a bigger role by modeling the liquid films in annular flow for fuel rod geometries including spacers e.g. [2]. The CFD models need to be validated with high-resolved experimental data, preferably in flow conditions similar to a BWR. Under BWR conditions a highly resolved instrumentation is however expensive and challenging, such that the validation of the model under similar conditions contains a high uncertainty. This is often the motivation to perform adiabatic experiments at conditions close to ambient pressure and temperature that are easier to instrument. A CFD approach based to a large extend on fundamental models, which can be used for flow modeling under BWR conditions, has to be also able to reproduce such adiabatic tests, when parts of the model describing processes connected to phase transition are switched off. Such a model can be trusted better if the validation is based on a wide base of different flow parameters and geometries.

In literature there are different physical based approaches to model annular flow:

- Fully resolved multiphase CFD calculation on basis of Direct Numerical Simulations (DNS) or Large Eddy Simulations (LES) by implementing surface tracking techniques, like Level-Set-Functions or the Volume-of-Fluid (VOF) method
- A one-dimensional prediction model, usually based on a gas-film-droplet three fluid approach.
   The mass and momentum transfer is either based on phenomenological or empirical correlations.
- A fully resolved single phase CFD calculation for the gaseous phase. Droplets and the liquid film are implemented by additional transport models, based on the CFD calculation.

DNS and LES approaches are expected most accurate to predict the complex flow in spacer proximity, the computational cost is however impractical for spacer development and therefore not found in literature. In the one-dimensional approach, the functional spacer has to be represented by empirical correlations, which can be obtained by experiments only. The only practical way to support spacer optimization is the application of CFD to determine the effect of the spacer to the velocity field in the gas core of the annular flow and couple it to a liquid film model.

Among the one-dimensional prediction models, the model of Kishore [10] is one of the few authors who apply it to non-equilibrium conditions. Among the authors, who model the liquid film as a two-dimensional distribution on the wall based on a fully resolved single phase CFD, Tso [13] is one of the first. Bai [3] and Adechy [1] take similar approaches.

The aim of our work is going into a similar direction like Adechy's model, however implemented in a simplified form. The goal was to create a simple RANS based model to predict the liquid film thickness and the corresponding liquid mass flow rates as a two-dimensional distribution around the fuel rod in the presence of a complex three-dimensional flow in the gas core behind a spacer. The modeling approach is tested with a quite wide database of experiments conducted in a double-subchannel flow geometry.

### 1. Experiments

#### 1.1 Facility

The experiments were conducted in the experimental facility CALVIN (Figure 1). At the heart of this facility is the vertical test section, shaped as double subchannel (Figure 2), through which the gas-water flow is conducted in co-current upward direction. The gas is circulated through the facility by a side channel compressor, while the water is fed by a pump. The water is injected directly as film onto the wall by a small gap of 0.5 mm around the test section profile at the bottom of the test section. Behind the test section the water and gas are separated in a droplet separator and returned into the storage tank or, respectively, sent back to the compressor. A heat exchanger keeps the temperature of both fluids constant at 20°C. The fact that the gas is circulated within the facility and is shut off from the environment by a water lock enables to run the experiments with different gases.

The test section has a total length of 2.5 meters. All elevations are given relative to the height of the gas inlet (0 mm): The water injection is located at a height of 500 mm. The sensitive area of the liquid film sensor (LFS) is around one of the half cylinders of the double subchannel between the elevation of 2200 mm to 2326 mm. Upstream of the water inlet, the channel has a square cross-section of 50 x 50 mm. Starting from the water injection device the channel shape changes to the double subchannel geometry, as shown in Figure 2.

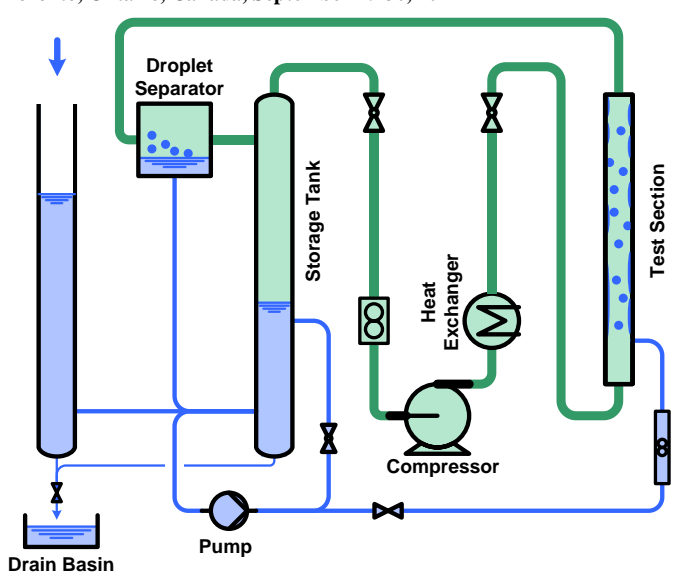


Figure 1 Schematic of experimental facility CALVIN

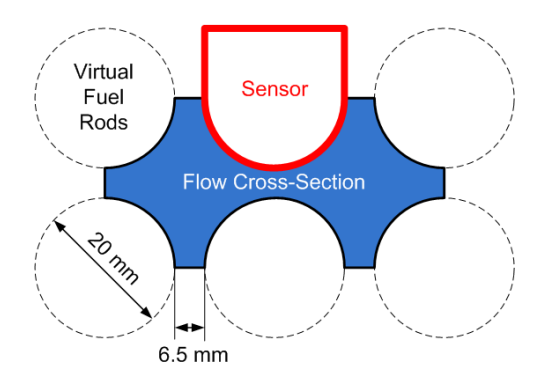


Figure 2 Double subchannel geometry of the test section

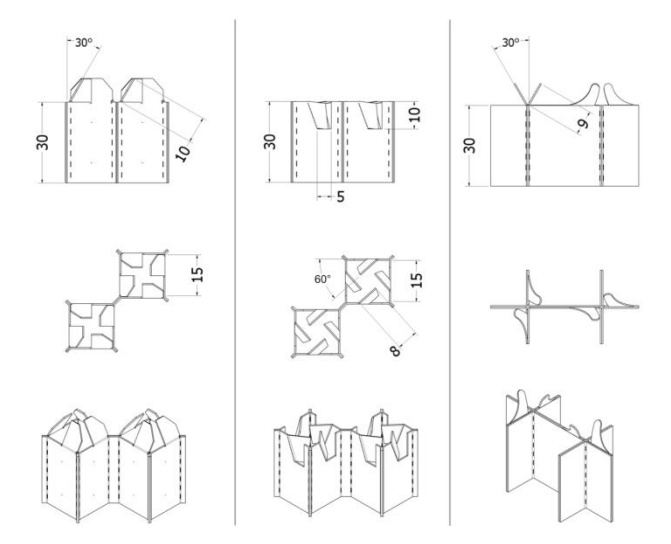


Figure 3 Spacer shapes Sp1 (left), Sp2 (center), Sp3 (right).

The length scale of the shape of the crosssection of the double subchannel is doubled compared to the subchannel of a real BWR. The flow conditions in the experiments would only be directly comparable with BWR conditions, if dimensionless numbers like e.g. Revnolds and Weber numbers are equal. They can only be matched in experiments under reactor conditions of a BWR, since densities, viscosities and surface tension change with different tendencies when pressure and temperature are increased. The up-scaling of the test section by a factor of two is therefore not of any disadvantage as it simply magnifies the length scales of the flow structures. Three different spacer shapes (Sp1, Sp2 and Sp3) were used for the experiments (Figure 3). Sp1 is a generic spacer while Sp2 and Sp3 are similar to spacers used in industrial applications [5; 12]. Experiments were performed for each spacer shape plus one reference experiment without spacer, making up four geometry variants. Additionally, the vane angle was varied, whereas only results for one vane angle are included in the present paper. Each spacer is mounted in the test section such, that the upper edge of the spacer body has the same elevation as the lowest line of measuring points of the LFS sensitive area. In this way the development of the liquid film can be observed starting directly downstream of the spacer. In the representation of the results, the lowest line of the LFS sensitive area is referred to as 0 mm.

### 1.2 Liquid Film Sensor

The basic idea for the fast acquisition of time sequences of two-dimensional film thickness distributions is an array of electrode pairs mounted flush to the wall. When a voltage pulse is supplied to the first electrode (transmitter electrode) of each pair, a current flows to the second electrode (receiver electrode), that is kept at zero potential. The current is depending on the thickness of an electrically conducting liquid film covering both electrodes. The electrode pairs are arranged around a half cylinder with 20 mm diameter in a 64x16 matrix with a periodic pitch of 2 x 2 mm<sup>2</sup> corresponding to

 $12^{\circ}$  pitch around the circumference. The conductance between the electrode pairs is acquired with 10'000 fps and represents the liquid film thickness on the sensor surface. The measuring range of the film thickness stretches from 0 to 800 microns with a measurement accuracy of about 20 microns. The sensor alters the rod surface by the electrodes being raised roughly 30  $\mu$ m above the insulating parts. The increased roughness might lead to a slightly different liquid film flow. However there is no statistical change of the dynamic liquid film thickness behavior along the sensor. The affect is therefore expected to be low. Because the liquid film is fully covering the rod surface, contact angle effects are not present. Details about the sensor design can be found in [6; 7; 8].

### 1.3 Conditions

All experiments are conducted at a temperature of 20°C and a static pressure of about 1.1 bar at the LFS location, the pressure depending slightly on the velocities of the media. The liquid is tap water with an electrical conductivity of about 300  $\mu$ S/cm. The gas is either helium (He,  $\rho$ =0.18 kg/m³), air ( $\rho$ =1.28 kg/m³) or octofluorocyclobutane (C<sub>4</sub>F<sub>8</sub>,  $\rho$ =9.41 kg/m³). All possible combinations of the three parameters total volume flux, gas and spacer shape were varied within the constraints of the experimental setup and the boundaries of annular flow towards other flow regimes (Table 2). The liquid volumetric flux ratio was kept constant at a value of 0.002.

Total volume flux J [m/s] 10 20 50 60 Air, C<sub>4</sub>F<sub>8</sub> He, Air, C<sub>4</sub>F<sub>8</sub>  $\overline{\text{He}}$ , Air,  $C_4F_8$  $C_4F_8$ He. Air no Sp Air He, Air, C<sub>4</sub>F<sub>8</sub> Sp1  $C_4F_8$ Air, C<sub>4</sub>F<sub>8</sub> Air,  $C_4F_8$ Air Air Sp2  $C_4F_8$ Air,  $C_4F_8$ He, Air,  $C_4F_8$ He, Air,  $C_4F_8$ He, Air Air Sp3  $C_4F_8$ Air,  $C_4F_8$ He, Air,  $C_4F_8$ He, Air,  $C_4F_8$ He, Air Air

Table 1 Experimental matrix

For all experiments, film thickness distributions were measured with a rate of 10'000 frames per second over a period of 10 seconds. With this high time resolution, it is actually possible, to capture the dynamics of the liquid film, e.g. all different properties of wave shape and movement. Since the modeling is aimed to model time-averaged liquid film thickness, the data is not shown time-resolved in this work. For a look on time-resolved data the reader is referred to [9].

#### 2. Numerical Scheme

The basic idea of the model is based on a single-phase Reynolds-Averaged-Navier-Stokes (RANS) CFD calculation of the gaseous phase. At the surface of the fuel rods, a non-slip boundary condition is posed to the gas flow field, whereas in reality there is a coupling to the velocity at the gas-liquid interface. The information of the wall shear stress from the RANS calculation is used to simulate the liquid film thickness and mass flow rate distribution by solving a two-dimensional transport equation for the liquid phase externally of the CFD code (Figure 4).

In the RANS calculation of the gas bulk flow neither the liquid film nor the droplets contained in the gas core are taking into account. Both, the restriction of the cross section by the presence of the liquid film and the influence of the gas-liquid interface on the turbulence in the gas bulk flow are neglected because of these simplifications. Neglecting furthermore droplet entrainment and deposition, the liquid is transported only by the shear forces acting from the side of the gaseous flow on the gas-liquid interface.

The liquid film thickness and mass flow distribution is described with a basic conservative mass transport equation (Equation 1)

$$\frac{\partial m}{\partial t} + \frac{\partial (mu_x)}{\partial x} + \frac{\partial (mu_y)}{\partial y} = 0 \tag{1}$$

The velocities  $u_x$  and  $u_y$  are defined in a coordinate system that stretches along the bended surface of the fuel rod model, where x is the coordinate in axial direction and y the one in lateral (or circumferential) direction. Curvature is neglected. Both velocity components are a function of the wall shear stress vector given by the gaseous phase. By assuming a laminar velocity profile in the liquid film perpendicular to the wall,  $u_x$  and  $u_y$  can be calculated by means of Equation 2. Gravity is neglected, which is a wide-spread approach for annular flow e.g. [14].

$$\tau = -\mu \frac{\partial u}{\partial z} \tag{2}$$

The shear du/dz is extracted from the single phase CFD calculation. With this information at hand the mass transport equation can be solved around the virtual fuel rod on a two-dimensional grid if the boundary conditions are known.

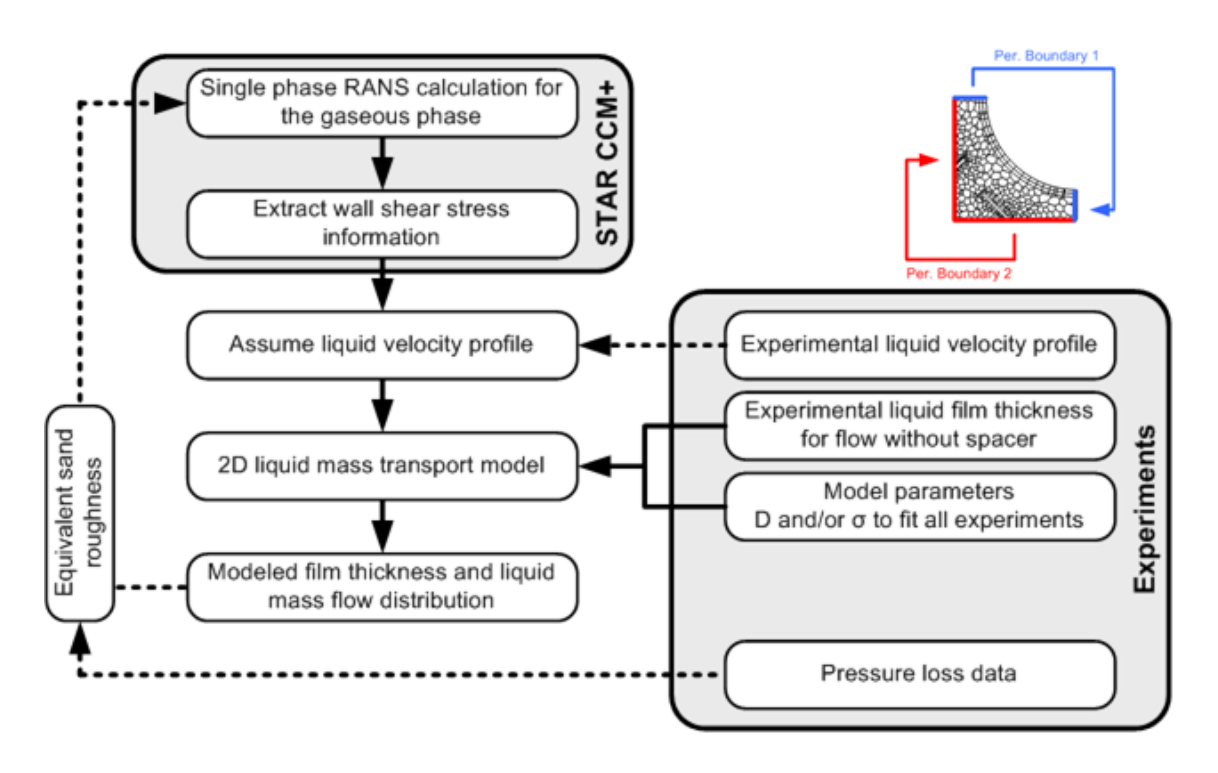


Figure 4 Schematic of liquid film model and boundary conditions of flow domain

The single phase RANS calculation is performed with the commercial code STAR-CCM+®. The calculation is carried out on an unstructured polyhedral mesh with an approximate cell diameter of 2 mm, the so called base size (Figure 5). In close proximity to the spacers the mesh size is reduced. The wall treatment in the code is conducted with a high Re-number approach, to save computational cost. For the same reason the k-ε-turbulence model was chosen. A mesh-size study was performed showing that the chosen mesh-size is not sufficient for an independent solution. The missing independency however is proven not to alter the good performance of the model in principal. The deficiency can actually be

compensated for partially by adjusting the model parameter in the liquid film model, with the purpose to save computational cost. A sensitivity study on the turbulence model is shown later in the work. Unlike the experiment, the subchannel is considered to have a periodic condition in all subchannel gaps. In the experiment this is only true in the gap between the pair of modeled subchannels. With this periodicity, a sufficient simulation domain is a quarter subchannel with periodic boundary conditions. With this difference between the experimental and simulation domain the computational cost is reduced substantially for Sp1 and Sp2, because Sp 1 and Sp 2 are 90°-periodic. A sensitivity analysis showed that apart from the corners in the experimental subchannels there is no significant difference between the periodic and real boundary simulation.

After a steady-state solution in the RANS is reached, the wall shear stress on the model fuel rod is read-out and saved into an external table. This table is read-in by a Matlab<sup>®</sup> routine and interpolated onto a Cartesian mesh with a base size of 2 mm, which stretches over the curved surface of the fuel rod model neglecting its curvature.

The heart of the Matlab<sup>®</sup> routine is the liquid mass transport equation (Equation 1), which is transferred by a Reynolds-Averaging-approach into Equation 3 by splitting the mass per occupying area and the velocity into a time averaged  $\overline{m}$ ,  $\overline{u}$  and a fluctuating part m', u'.

$$\frac{\overline{\partial(\overline{m}+m')}}{\partial t} + \frac{\overline{\partial((\overline{m}+m')(\overline{u}_x + u'_x))}}{\partial x} + \frac{\overline{\partial((\overline{m}+m')(\overline{u}_y + u'_y))}}{\partial y} = 0$$
 (3)

Simplification and the application of averaging rules results in Equation 4

$$\frac{\partial \overline{m}}{\partial t} + \frac{\partial (\overline{u}_x \overline{m})}{\partial x} + \frac{\partial (\overline{u}_y \overline{m})}{\partial y} + \frac{\partial (\overline{u'_x m'})}{\partial x} + \frac{\partial (\overline{u'_y m'})}{\partial y} = 0$$
 (4)

In a similar way as the Reynolds Averaging of the Navier-Stokes-Equation is performed, the Boussinesq hypothesis is chosen to model the nonlinear fluctuating terms with a diffusion equation:

$$\frac{\partial \overline{m}}{\partial t} + \frac{\partial (\overline{u}_x \overline{m})}{\partial x} + \frac{\partial (\overline{u}_y \overline{m})}{\partial y} - D \left( \frac{\partial^2 \overline{m}}{\partial x^2} + \frac{\partial^2 \overline{m}}{\partial y^2} \right) = 0$$
 (5)

Integrating Equation 2 results in Equation 6 by converting the considered volume of the liquid film into mass and considering a no-slip-condition for the liquid at the wall ( $u_i$  denotes any of both components of the velocity on the interface).

$$\bar{u}_i = \frac{\bar{\tau}_i H}{2\mu_l} \tag{6}$$

The dependency between film thickness and mass inventory of a considered volume of the liquid film is described by Equation 7.

$$m = H\rho_1 \tag{7}$$

Combining Equations 5, 6 and 7 leads to the final transport equation:

$$\rho_{l} \frac{\partial H}{\partial t} + \frac{\partial}{\partial x} \left( H^{2} \tau_{x} \frac{\rho_{l}}{2\mu_{l}} \right) + \frac{\partial}{\partial y} \left( H^{2} \tau_{y} \frac{\rho_{l}}{2\mu_{l}} \right) - D \frac{\partial^{2}}{\partial x^{2}} (H \rho_{l}) - D \frac{\partial^{2}}{\partial y^{2}} (H \rho_{l})$$

$$= 0$$
(8)

Equation 8 can be interpreted as the transport of the film thickness in two dimensions by a field function of the shear stress based on the conservation of mass. The transport equation is implemented as upwind finite element scheme.

The film thickness at the channel inlet is known from the time-averaged film thickness of the experiments without spacer and fed as boundary condition into the numerical scheme. The film thickness distribution around the fuel rod is nearly uniform in the absence of a spacer grid. Therefore a constant film thickness is assumed around the circumference.

For the outlet it is assumed that the film thickness is constant in axial direction, which is justified if the gradient of the shear stress in this direction goes towards zero. This is the case if the simulation domain is chosen correctly, far away from the spacer. For the sides of the simulation domain a periodic boundary is chosen, as this corresponds to the boundary of the CFD simulation domain.

The diffusion coefficient D, being introduced by the Boussinesq assumption in the film model for the additional mass transport, is the only modeling parameter in the presented model. In a classical Reynolds-Averaging approach the diffusion coefficient is a function of the location. It depends on the local turbulence characteristics calculated by the turbulence model. In this work the coefficient is chosen constant independent of the location. Further it is kept constant across all flow conditions. The reason is the unknown relationship between the turbulent viscosity of the gaseous phase and the turbulent mass diffusion of the liquid film, which could be coupled by a turbulent Schmidt number. There is however potential for future model improvements.

#### 3. Results

### 3.1 Comparison of Time-Averaged Film Thickness

Figure 5 shows a direct comparison between experiments and simulation of the liquid film distribution for different spacers and gases at a total volume flux of 30 m/s. Figure 6 shows the lateral film thickness profile at a position 30 and 90 mm downstream of the spacer for the three different spacers of an air-water flow.

The figures show that for all spacers and gases the model predicts well the accumulation of liquid into streaks. This concerns the position of the streaks on the model fuel rod as well as the absolute value of the liquid film thickness.

For Sp1 the model has a good agreement with the experiments concerning the position of the streaks downstream of Sp1 over the whole sensor length. Furthermore the minimum film thickness, which is in its dependency with the mass flow rate an important parameter in regard to dryout, is well predicted (Figure 6). The diffusion coefficient (D=3e5) in the model is too big for all gases between 60 to 120 mm downstream of the spacer, as the streak is smeared out too strong in lateral direction compared to the experiment. A decrease of the diffusion coefficient however would lead to sharper gradients in the spacer proximity, which are still too big with the chosen diffusion coefficient. A diffusion coefficient which is dependent on the location or, respectively, on local turbulence quantities, analogue to the turbulent viscosity in a turbulence model, might be able to overcome this deficiency. For Sp2 the model brings comparably good results as for Sp1, the lateral swing back motion of the streak from the right to the left channel seen in the experiment is however not reproduced in the model. A sensitivity study showed, that neither the turbulence model nor the periodic boundary in the subchannel gap are the reason for this discrepancy between experimental and simulation results. The flow downstream of Sp3 is well predicted within the first 50 mm downstream of the spacer. The accumulation of liquid in the left subchannel from 60 mm onwards as seen in the experiments is not predicted by the model, independent of the gas. A sensitivity study showed that as for Sp2 neither the turbulence model nor the periodic boundary in the subchannel gap are the reason for this discrepancy. Most probably this accumulation is due to a formation of roll waves. This complex strongly timedependent interaction at the gas-liquid interface is not reflected by the simplified modeling approach and can therefore cause significant deviations.

Figure 7 shows that the model predicts the film thickness also quite well for different total fluxes. The major contribution for the good performance is the very accurate initial film thickness received from the experiments without spacer.

In general the model yields satisfying results as the most important flow phenomena are captured, namely the accumulation of liquid in streaks and their transport downstream of the spacer. The absolute film thickness is usually predicted in the right order of magnitude. The minimum film thickness, which is in its dependency with the mass flow rate an important parameter concerning dryout, is in most cases modeled with an accuracy better than 50 microns. The diffusion coefficient is the essential key factor to predict the lateral film thickness gradients correctly.

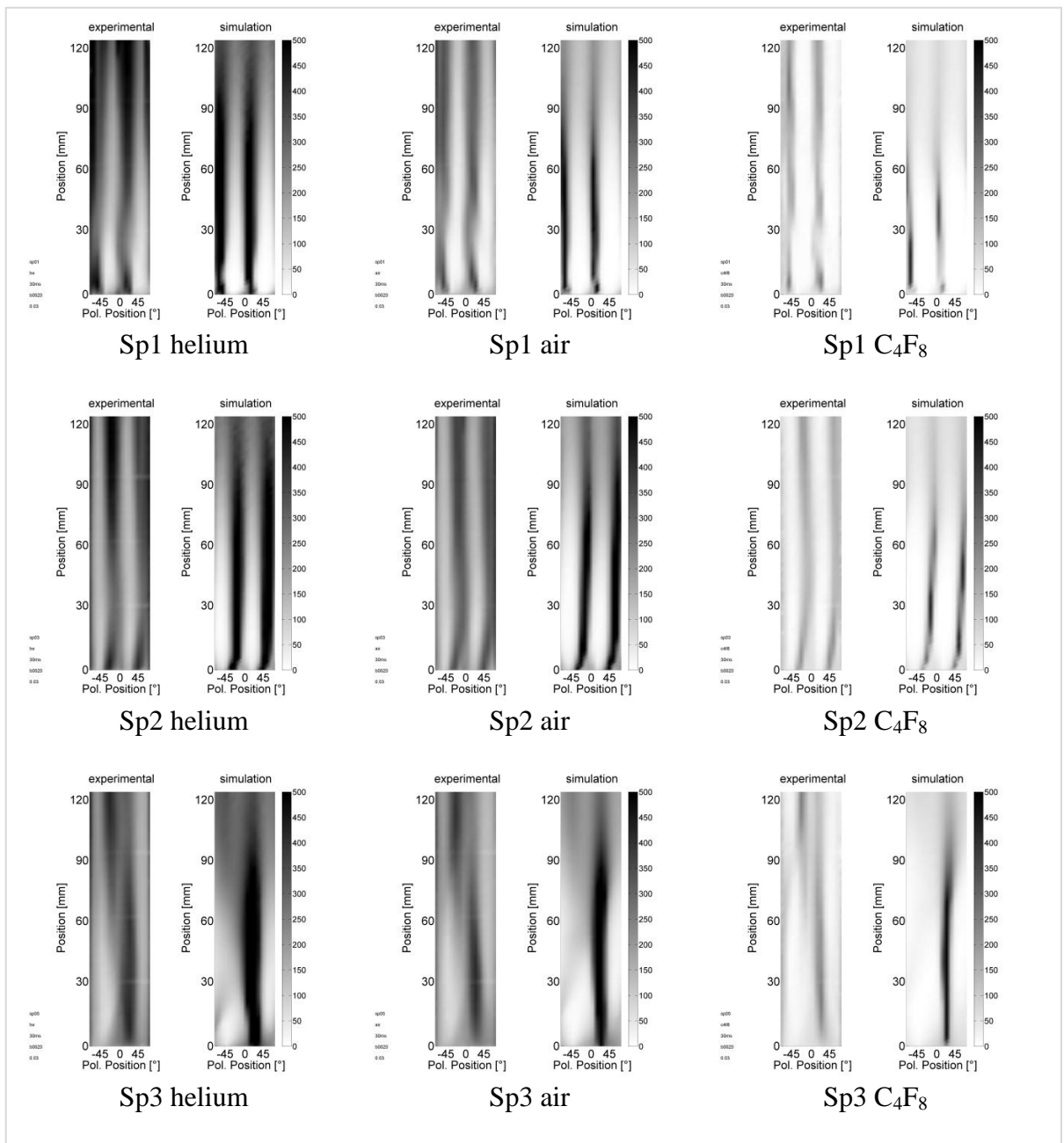


Figure 5 Experimental and simulated film thickness at J=30m/s and 1-b=0.002 for different spacer geometries and gases (diffusion coefficient 3e5)

### 3.2 Sensitivity Study of the Model

As pointed out in the previous paragraphs, different parameters and assumptions have to be made for the successful modeling of the liquid film in three-dimensional flows. The strength of their influence can be estimated by a sensitivity analysis. With the sensitivity analysis the key parameters and limits of the model are better understood. Furthermore it enables to direct the focus of future research into the most promising direction.

The sensitivity analysis shown in this work treats following parameters:

- Liquid mass transport equation
- Velocity profile in the liquid film
- Turbulence model of the RANS simulation

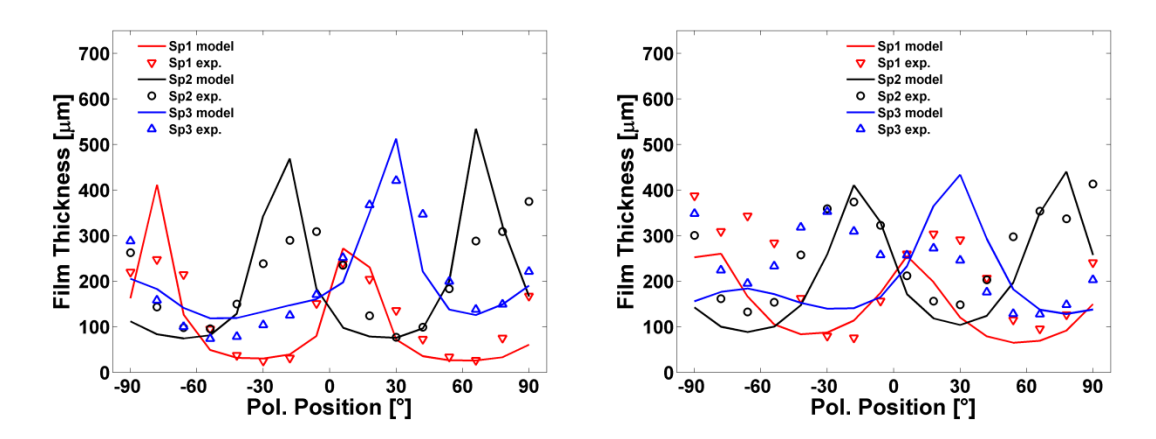


Figure 6 Simulated and experimental lateral liquid film thickness distribution for different spacers (J=30m/s, air, Position 30mm (top) and 90 mm (bottom))

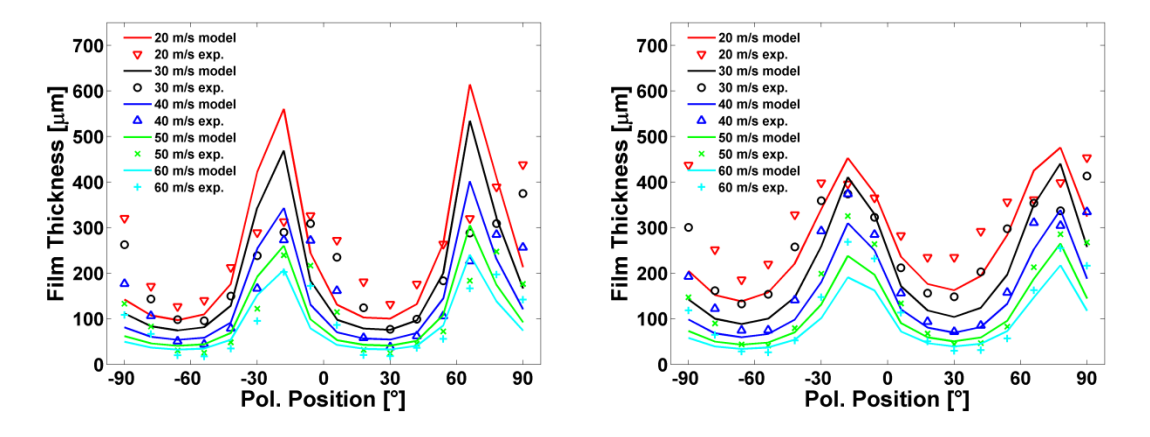


Figure 7 Simulated and experimental lateral liquid film thickness distribution for total volume fluxes ( Sp 2, air, Position 30mm (top) and 90 mm (bottom))

#### **Mass Transport Equations**

The local thinning and accumulation of the liquid film is the result of two different flow mechanisms:

- 1. Increase and decrease of the local shear magnitude: The liquid film thickness decreases by the increased shear magnitude at the interface, increasing the liquid film velocity. This effect does not influence the local liquid mass flow rate.
- 2. Two-dimensional liquid mass redistribution because of diverging or converging wall shear stress: This reduces or increases the local liquid mass flow rate and therefore also the liquid film thickness.

With the liquid film sensor, as used in the experiments of this work, the weighting between the two mechanisms cannot be determined. This however is crucial for the prediction of dryout, which is basically only dependent on the liquid mass flux.

An option to adjust the liquid film transport equation is to neglect lateral shear forces, as it is done for the one-dimensional models.

Figure 8 (b) shows the results if only the local wall shear stress magnitude is taken into account, implying a constant mass flow distribution around the rod. This leads to a strong overprediction of the liquid film thickness compared to the experimental result (Figure 8a). It can therefore be concluded that an increase of the film velocity due to interfacial shear alone cannot be the major cause of the local thinning and accumulation of the liquid. Only the redistribution of the liquid mass flux around the model rod can explain the time-averaged liquid film thickness distributions in the presence of spacers. The numerical scheme represented by Equation 8 contains the Boussinesq approximation for the fluctuating terms, which is a widely used approach in fluid dynamics. The importance of the diffusion term becomes evident in Figure 8 (c). The figure shows the liquid film distribution without diffusion term. It can be seen that the diffusion term helps to reproduce the lateral streak curvature as it is seen in the experiments (Figure 8d). However without the diffusion term there is still a good qualitative agreement between model and experiments, namely the structure of the liquid film into streaks.

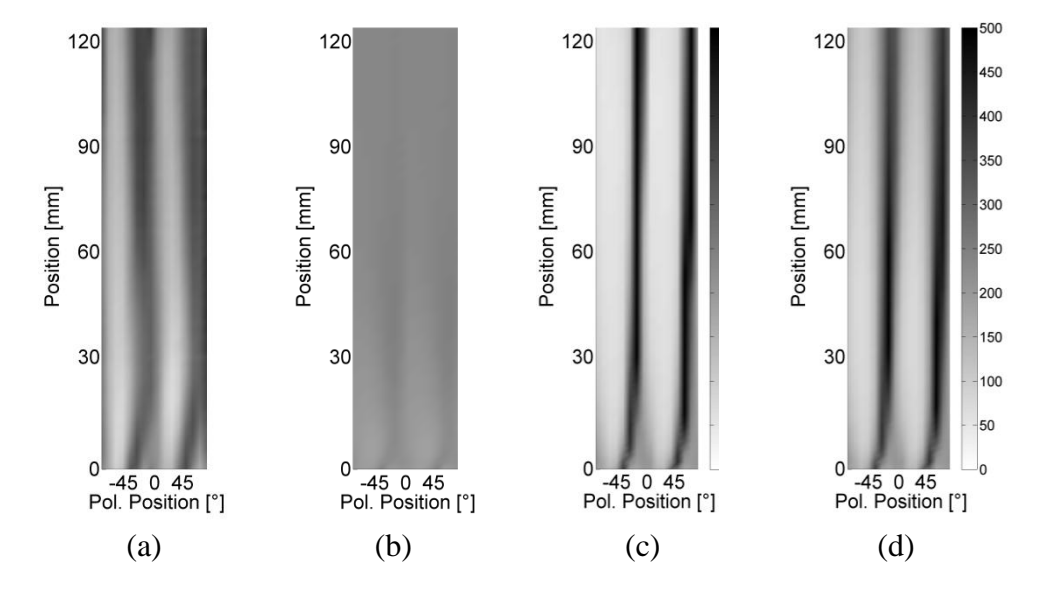


Figure 8 Influence of liquid film modeling equation (J=30m/s, Sp 2, air). (a) experimental,

- (b) one-dimenional model,
  - (c) no diffusion,
  - (d) with diffusion

#### Velocity profile

A core assumption of the numerical scheme presented above is the laminar velocity profile in the liquid film perpendicular to the wall. This assumption is most probably inaccurate.

The best velocity profile for the model of this work is not clear. The reason is that the transported mass flux is the integral of the profile of the liquid superficial velocity. This profile is a strong function of the wave pattern and wave velocity, which are physically hard to predict with simple modeling. The simple approach of taking a laminar velocity profile however yields, as shown in the previous paragraph, good results, even though from a physical point of view it might only partially reflect reality. In order to check the sensitivity of the results to the velocity profile in the film, three different velocity profiles were checked:

- Laminar velocity profile
- Block velocity profile
- Logarithmic portion of the law-of-the-wall turbulent velocity profile

The block velocity profile is defined as constant velocity perpendicular to the wall scaling linear with the wall shear stress. Because the block velocity profile neglects the no-slip boundary condition at the wall it is far away from reality. It can be considered as extreme towards maximal mass transport in very thin liquid films.

The sensitivity study showed that the laminar velocity profile actually performs best compared to the other velocity profiles. This might be surprising, because the laminar velocity profile is very different to the real velocity profile which is the product of the law-of-the-wall with the time-averaged liquid holdup. But for the liquid film model proposed in this work, it is actually not relevant, if the real velocity profile is fed into the equation. It is on the other hand crucially important that the dependency between the integral of the real velocity profile and the integral of the assumed velocity profile behaves linear for all interfacial shears present in the flow. The reason is that the shear is connected with the experimental liquid film thickness at the domain inlet. If the dependency is linear between the integral of the assumed and real velocity profile, the film thickness is predicted correctly in the whole simulation domain.

The superior performance of the laminar film velocity profile in the liquid film model gives a hint that in reality the transported liquid mass scales roughly with the quadratic wall shear stress created by the gas shear.

#### **Turbulence Model**

Among the most used turbulence models in commercial CFD codes, it is considered best practice that a Reynolds-Stress turbulence model (RSM) is used for complex three-dimensional flows. RSMs however are significantly more expensive from a computational point of view than two-equation-models like e.g. the k-\varepsilon-model.

The sensitivity study showed that the modeled film is hardly influenced by the turbulence model, in case of the flow around Sp2, because the difference between the RSM and the k-ε- model is marginal. The insignificance of the turbulence model downstream of spacer has been reported earlier: [4] actually discovered a superior performace of the k-ε-model compared to the RSM for spacer flows at least under single phase conditions.

#### 4. Conclusion

A simple model for the prediction of liquid film thickness and mass flow rate distributions in the presence of complex three-dimensional annular flows is suggested. It is based on a single phase RANS CFD calculation for the gas core. From the CFD results the wall shear stress stresses are extracted and used to model the two-dimensional transport of the liquid film on the channel wall. The model is a

simplified form of Adechy's [1] and Bai's [3] model and designed for flows with strong interfacial shears. A new feature is the modeling of wall shear stress fluctuations and their influence on the liquid film distribution by means of a Boussinesq approximation. This approximation introduces the liquid mass diffusion coefficient as the only model coefficient.

The model is validated against highly resolved film thickness measurements in a double subchannel geometry of a BWR mockup with spacers. The flow parameters varied are the flow obstacles (spacers), gas density and total volume flux.

The results show good agreement for the right choice of the model coefficient. A sensitivity analysis is performed, to make apparent the strength and weaknesses of the proposed model for flows behind flow obstacles. The results can be summarized as follows:

- A two-dimensional mass transport in the liquid film together with the Boussinesq approximation for treating fluctuations of the driving shear stresses created by the gas flow is sufficient to get in the right orders of magnitude for the film thickness distribution. The model underlines the fact, that the thinning of the liquid film downstream of spacers is mostly caused by a redistribution of liquid flux around the fuel rod in lateral direction.
- The turbulence model in the RANS CFD is of minor influence.
- The velocity profile assumed for the liquid film plays a minor role, as it is always relative to the velocity profile at the domain inlet.
- The diffusion coefficient is the only model parameter, which might be modeled in the future in dependency on flow conditions and turbulence information of the single phase RANS.

#### 5. References

- [1] Adechy, D. and R. I. Issa (2004). "Modelling of annular flow through pipes and T-junctions." Computers & Fluids **33**(2): 289-313.
- [2] Azuma, M. (2005). "Numerical Simulation on Liquid Film Behaviors in BWR Fuel Bundle geometry using the VOF Method." <u>13th International Conference on Nuclear Engineering</u>, Beijing, China, May 16-20, 2005 **ICONE13-50162**.
- [3] Bai and Gosman (1996). "Mathematical modeling of wall films formed by impinging sprays." S.A.E. Transactions **6**: 782-796.
- [4] Conner, M. E., E. Baglietto, et al. (2010). "CFD methodology and validation for single-phase flow in PWR fuel assemblies." <u>Nuclear Engineering and Design</u> **240**(9): 2088-2095.
- [5] D'Orio (1998). "Patent No.: US 5,790,624." United States Patent.
- [6] Damsohn, M. and H. M. Prasser (2009). "High-speed liquid film sensor for two-phase flows with high spatial resolution based on electrical conductance." Flow Measurement and Instrumentation **20**(1): 1-14.
- [7] Damsohn, M. and H. M. Prasser (2009). "High-speed liquid film sensor with high spatial resolution." Measurement Science and Technology(11): 114001.
- [8] Damsohn, M. and H. M. Prasser (2010). "Experimental studies of the effect of functional spacers to annular flow in subchannels of a BWR fuel element." <u>Nuclear Engineering and Design</u> **240**(10): 3126-3144.
- [9] Damsohn, M. and H. M. Prasser (2010). "Experimental studies of the effect of functional spacers to annular flow in subchannels of a BWR fuel element." <u>Nuclear Engineering and Design</u> **In Press, Corrected Proof**.

- [10] Kishore, B. N. and S. Jayanti (2004). "A multidimensional model for annular gas-liquid flow." Chemical Engineering Science **59**(17): 3577-3589.
- [11] LeCorre, J.-M. and C. Adamsson (2008). "Validation of a Mechanistic Tool for the Prediction of Critical Power BWR Fuel Assemblies." <u>NUTHOS-7: The 7th International Topical Meeting on Nuclear Reactor Thermal Hydraulics, Operation and Safety, Seoul, Korea.</u>
- [12] Nylund (2004). "Patent No.: US 6,816,563,B2." <u>United States Patent</u>.
- [13] Tso, C. P. and S. Sugawara (1990). "Film thickness prediction in a horizontal annular two-phase flow." <u>International Journal of Multiphase Flow</u> **16**(5): 867-884.
- [14] Wolf, A., S. Jayanti, et al. (2001). "Flow development in vertical annular flow." <u>Chemical</u> Engineering Science **56**(10): 3221-3235.